POLITECNICO DI TORINO
Repository ISTITUZIONALE

Singular Higher-Order Complete Vector Bases for Finite Methods

Original
Singular Higher-Order Complete Vector Bases for Finite Methods / Graglia, R., Lombardi, G.. - In: IEEE TRANSACTIONS ON ANTENNAS AND PROPAGATION. - ISSN 0018-926X. - STAMPA. - 52:7(2004), pp. 1672-1685. [10.1109/TAP.2004.831292]

Availability:
This version is available at: 11583/1401750 since:

Publisher:
IEEE

Published
DOI:10.1109/TAP.2004.831292

Terms of use:

This article is made available under terms and conditions as specified in the corresponding bibliographic description in the repository

Publisher copyright

(Article begins on next page)

28 November 2026

Singular Higher Order Complete Vector Bases for Finite Methods

Roberto D. Graglia, *Fellow, IEEE,* and Guido Lombardi, *Member, IEEE*

***Abstract*—This paper presents new singular curl- and divergence-conforming vector bases that incorporate the edge conditions. Singular bases complete to arbitrarily high order are described in a unified and consistent manner for curved triangular and quadrilateral elements. The higher order basis functions are obtained as the product of lowest order functions and Silvester–Lagrange interpolatory polynomials with specially arranged arrays of interpolation points. The completeness properties are discussed and these bases are proved to be fully compatible with the standard, high-order regular vector bases used in adjacent elements. The curl (divergence) conforming singular bases guarantee tangential (normal) continuity along the edges of the elements allowing for the discontinuity of normal (tangential) components, adequate modeling of the curl (divergence), and removal of spurious modes (solutions). These singular high-order bases should provide more accurate and efficient numerical solutions of both surface integral and differential problems. Sample numerical results confirm the faster convergence of these bases on wedge problems.**

***Index Terms*—Electromagnetic analysis, electromagnetic scattering, finite element methods (FEMs), Galerkin method, high-order modeling, method of moments (MoM), numerical analysis, singular vector functions incorporating edge conditions, wedges.**

I. Introduction

NUMERICAL methods using subsectional high-order vector bases are nowadays able to deal with very complex electromagnetic structures. The finite element method (FEM) can be used to discretize partial differential models of isotropic or anisotropic inhomogeneous media, and use of high order vector expansion functions of the curl-conforming kind suppresses nonphysical spurious modes from the numerical solution [1]–[3]. Similarly, the method of moments (MoM) can be applied to discretize integral equation models of metallic structures by using high-order vector functions of the divergence-conforming kind (see for example [1]).

Numberless structures of practical engineering interest contain conducting or penetrable edges and, in the vicinity of these edges, the surface charge [4]–[6] and the field behavior can be singular [6]–[9]. Unfortunately, though the singular behavior of the electromagnetic field or current can be quantitatively appreciated only at the edge extreme, one needs to use more expensive, very dense meshes in the neighborhood of the edges in order to model the fields, even though high-order vector bases are in use.

In general, it is not granted that *iterative mesh refinement* could provide good effective solutions to these problems, whereas iterative mesh refinement involves complex procedures and codes, uses additional unknowns and it usually results in an increase of the computational time and/or memory requirements. The literature shows that iterative mesh-refinement is widely used in the FEM context (see, for example, [10]), whereas it can hardly be considered by MoM practitioners since MoM matrices are not sparse and one would have to recompute too many matrix coefficients for any new refined mesh. Incidentally, in this connection, we notice that in the neighborhood of an edge the commonly used testing techniques are questionable, and use of different weight functions could improve the convergence of the numerical results [11], [12].

The best alternative to heavy mesh refinement or to using very dense meshes is the introduction of singular functions able to precisely model the singular edge behavior of fields and currents. As far as the FEM treatment of edge singularities is concerned, important contributions to the development of scalar and vector expansion functions incorporating the singular behavior are provided in [13]–[20], whereas the continuous interest in incorporating edge conditions in MoM solutions dates back to the mid seventies of last century [21], with more recent contributions available in [22]–[24]. This topic has obviously been considered by other finite methods, and the interested reader can for example refer to [25]–[30]. Entire-domain basis functions modeling of edge singularities has been addressed in [31], [32], for example, though this seems to have less general applicability.

This paper presents new curl- and divergence-conforming singular, high-order vector bases on curved two-dimensional (2-D) domains. The bases are directly defined in the parent domain without introducing any intermediate reference frame, differently to what has been done by other authors [13], [18], [19]. Our bases incorporate the edge conditions and are able to approximate the unknown fields in the neighborhood of the edge of a wedge for any order of the singularity coefficient ν, that is supposed given and known *a priori*. The wedge can be penetrable in the curl-conforming case, while it is supposed impenetrable (metallic) in the divergence conforming case.

To introduce the material that follows it is of importance to first recognize that the geometrical and material discontinuity introduced by a wedge yields to a 2-D problem, since in the near-edge region any edge can be considered as straight [6]. One has then to separately consider the models to deal with

Manuscript received April 3, 2003; revised August 8, 2003. This work was supported by the Italian Ministry of Education, University and Research (MIUR) under the Fund for Investments in Basic Research (FIRB) Grant RBAU01M9PF: *Vector expansion functions for singular fields*. Patent protection of this work has been applied for in Italy, and extension of patent coverage in other countries is being considered.

R. D. Graglia and G. Lombardi are with the Dipartimento di Elettronica, Politecnico di Torino, 10129 Torino, Italy (e-mail: roberto.graglia@polito.it, guido.lombardi@polito.it).

Digital Object Identifier 10.1109/TAP.2004.831292

0018-926X/04$20.00 © 2004 IEEE

the singularity of the current from those used to deal with the singularity of the electromagnetic fields. Discretization of the current is required by the MoM solution of surface integral equations; conversely, discretization of the electric $(\boldsymbol{E})$ or of the magnetic $(\boldsymbol{H})$ field is required by FEM approaches and, in the vicinity of an edge, this discretization involves a volumetric region.

To clarify the problem let us consider for a moment the fields at angular frequency ω in the neighborhood of a straight metal wedge of aperture angle α immersed in free space, with electric permittivity and magnetic permeability equal to ε_0 and μ_0, respectively. By introducing a polar reference frame (ρ, ϕ, z) with origin at the edge of the wedge and with the $\boldsymbol{z}$ axis parallel to the edge itself, the surface current $\boldsymbol{J}_s$ and the electromagnetic field in the vicinity of the edge assume, when expanded in series [6], [7], the following form (only the first terms are reported):

$$\boldsymbol{J}_s = \frac{\nu A}{\rho^{1-\nu}}\hat{\boldsymbol{z}} + j\omega\varepsilon_0 B\rho^{\nu}\hat{\boldsymbol{\rho}} \pm \text{constant}\ \hat{\boldsymbol{\rho}} \tag{1}$$

$$\begin{cases} E_z = j\omega\mu_0 A\rho^{\nu}\sin\nu\phi \\ \boldsymbol{H}_t = \frac{\nu A}{\rho^{1-\nu}}\left(\sin\nu\phi\hat{\boldsymbol{\phi}} - \cos\nu\phi\hat{\boldsymbol{\rho}}\right) \end{cases} \tag{2}$$

$$\begin{cases} H_z = j\omega\varepsilon_0 B\rho^{\nu}\cos\nu\phi + \text{constant} \\ \boldsymbol{E}_t = -\frac{\nu B}{\rho^{1-\nu}}\left(\cos\nu\phi\hat{\boldsymbol{\phi}} + \sin\nu\phi\hat{\boldsymbol{\rho}}\right) \end{cases} \tag{3}$$

where A and B are appropriate coefficients. The constant component in the radial part of the surface current, when present, does not pose any numerical modeling problem. This constant component vanishes for a zero-thickness metal edge and, as indicated, it has opposite sign on the two sides of the wedge since no charge accumulates at the edge. Equations (2) and (3) hold for the transverse magnetic (TM) and for the transverse electric (TE) part, respectively. For a perfectly conducting wedge of aperture angle α one has $\nu = \pi/(2\pi-\alpha)$. The smallest value of $\nu = 1/2$ occurs for a half-infinite plane $(\alpha = 0)$. Only the current component parallel to the metal edge and the transverse components of the electromagnetic fields can become infinite at the edge. The longitudinal magnetic field H_z could have a constant component, whereas both E_z and H_z have a component that at the edge vanishes as ρ^{ν}. Although the singularity coefficient ν depends on the geometry and on the wedge material properties, the previous expressions can be generalized to represent fields in the neighborhood of a wedge made of different penetrable or not-penetrable materials, provided the azimuthal dependence factors in (2) and (3) are adequately modified [6], [8]. Then, in general, the curl of the transverse fields contains a constant component since the curls of $\boldsymbol{E}_t$ and $\boldsymbol{H}_t$ are related to the longitudinal component H_z and E_z, respectively. The singularity coefficient of isotropic penetrable wedges is always greater than 1/2 [6]. The singularity coefficient ν is usually evaluated for the static case [8]. The singularity coefficient is frequency independent, and the coefficient of the dynamic case can be proven to be equal to the static case one [33].

The paper starts by defining singular lowest order vector bases, and by listing the four general requirements they have to fulfill. Section III then describes the element representation to derive singular curl-conforming bases on triangular and quadrilateral domains, with derivation of the high-order static potentials that permit one to systematically derive the static singular components of these bases. The new curl-conforming bases and their associated longitudinal bases are described in Section IV, whereas Section V reports the new divergence-conforming bases. Numerical FEM results to illustrate the benefits of using such new bases are reported in Section VI. Part of the material reported here was presented in [34]–[36].

II. Singular, Lowest Order Complete Vector Bases

A thorough investigation of the previous literature has shown that the fundamental question to be raised before deriving singular vector bases regards the number of basis functions required to define the *lowest order* bases. For example, the six basis functions given in [18], or the eight basis functions introduced in [19], define singular triangular elements compatible to first order curl-conforming elements adjacent to the element edge opposite to the singular vertex. Those bases are not of the lowest order since zeroth-order regular elements cannot be made adjacent to singular ones. As a matter of fact, for triangular curl-conforming elements, the lowest number of functions required to achieve completeness and singular conformity to adjacent first-order elements is proved in Section IV-A to be equal to eleven ($p = 1$, $s = 0$ order), whereas six vector functions are at least necessary for completeness and singular conformity to adjacent zeroth-order elements (order $[0,0]$).

We investigated several ways to derive *singular* and *complete* lowest order vector bases. We define singular bases to be lowest order complete when the following properties are fulfilled:

1) the basis set is complete just to the regular zeroth order, and for curl (or divergence) conforming bases the curl (divergence) of the bases is also complete to regular zeroth order;
2) the singular element is fully compatible to adjacent zeroth-order regular elements attached to its nonsingular edges, and to adjacent singular elements of the same order attached to the other edges;
3) the basis functions can model the static, $\rho^{\nu-1}$ singular behavior of the transverse electromagnetic fields (curl-conforming case), or of the surface current and charge density (divergence-conforming case), *in the neighborhood* of the wedge (first term of Meixner's series [7]), ρ being the radial distance from the wedge sharp-edge profile;
4) the curl-conforming bases are able to model a nonsingular transverse field with curl that vanishes at the edge of the wedge as ρ^{ν}, whereas the divergence-conforming bases can model the radial component of the current density that vanishes as ρ^{ν} at the wedge sharp-edge ($\nu \neq 1$ and not integer).

The second requirement is necessary to remove spurious numerical solutions. The first requirement has been introduced not to limit the size of the mesh in the neighborhood of the edge of the wedge. Above all, it permits one to deal with all cases where the singularity of the fields is not excited. To satisfy the first requirement the lowest order set must contain all the zeroth-order regular basis functions. Notice that by removing this requirement one can obtain singular interpolatory bases that exactly reduce to the standard (regular) bases in the limit for singularity coefficient $\nu = 1$ (see [38]).

Our lowest order bases are used to built higher order singular vector bases with a simple procedure. All our singular high-order bases contain the regular (polynomial) bases as one subset; hereafter these subsets are reported in interpolatory form, although they could also take hierarchical form. The other remaining (Meixner) subset of the complete bases could be constructed independently in hierarchical, interpolatory, or in other forms. This latter subset, named after Meixner because it models just the Meixner series, contains the singular terms as well as other nonsingular irrational algebraic (that is nonpolynomial) terms. The Meixner subset can be regarded as the irrational algebraic part of the complete bases.

In spite of the fact that the subset of the regular functions could have interpolatory form [1], the third and first requirement together prevent singular *complete* bases of interpolatory form to be constructed even at the lowest order. In fact, the regular and the Meixner subsets altogether cannot be interpolatory since they are used to represent on the same element both regular as well as irrational algebraic vector functions. One of the major results of this paper is that our new singular bases do not interfere with the interpolatory nature of the conventional bases eventually used on the regular elements attached to the singular ones.

In this connection, we observe that there is no reason to represent a singular behavior in terms of interpolation functions since the singular behavior is local in nature and proper only in the neighborhood of the edge of the wedge, with singularity coefficient ν that depends on integral properties of the solution, that is on energy considerations. The singularity coefficient ν must be known *a priori*. In all the problems where singular fields are not excited one numerically finds that the expansion coefficient associated with each singular expansion function is zero.

III. Element Representation and Sharp-Edge Potentials for Curl-Free Singular Fields

A local numbering scheme is used for parent variables, edges, height and edge vectors, and vertices of 2-D elements [1]. The edges of each triangular element are numbered counter-clockwise from 1–3, and the parent variable ξ_β (with $\beta = 1,2,3$) varies linearly across the element and vanishes on the βth edge, with $\xi_\beta = 1$ on the vertex opposite to edge β [1]. For this reason, the vertices of the triangle could be given the same local-order number already associated with their opposite edge. In the following, for all the elements attached to the sharp-edge vertex, we refer to these local numbers in terms of dummy indexes. In particular, with reference to Fig. 1, we locate on the sharp-edge vertex the ith vertex of each triangular sharp-edge element. The dummy index i can be equal to 1, 2 or 3 and index arithmetic is performed modulo three (that is $i + 1 = 1$ when $i = 3$). For each triangular sharp-edge element, the two edges $(i \pm 1)$ depart from the sharp-edge vertex, while the ith edge is opposite to the sharp-edge vertex.

Similarly, for quadrilaterals, the edges are numbered counter-clockwise from 1–4 and the parent coordinate ξ_β (with $\beta = 1$, 2, 3, 4) varies linearly across the element and vanishes on the βth edge, attaining a value of unity at the edge opposite to the $\xi_\beta = 0$ coordinate line [1]. In this case index arithmetic is performed modulo four. For quadrilateral sharp-edge elements, edge i and $i + 1$ are those departing from the sharp-edge vertex.

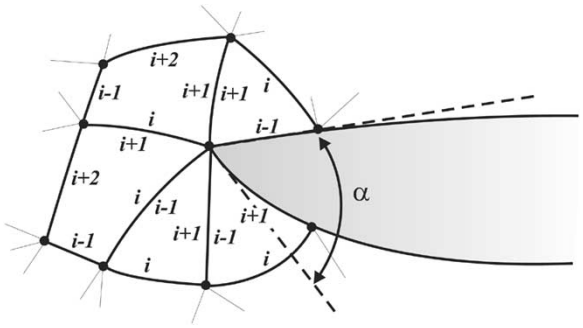


Fig. 1. Cross-sectional view of the region around a sharp, but curved edge of aperture angle α meshed with curved curl-conforming elements. The sharp-edge elements are those attached to the sharp-edge vertex and the figure shows a case with five sharp-edge elements. The edges of each element are locally numbered counter-clockwise from 1–3 for triangles, and from 1–4 for quadrilateral elements. For each sharp-edge element it is convenient to refer to these local numbers in terms of the dummy indexes $i - 1, i, i + 1, i + 2$, with index arithmetic performed modulo three for triangles ($i + 1 = 1$ if $i = 3$) and modulo four for quadrilaterals.

Fig. 1 shows that the local number for the side common to two attached triangles is $(i - 1)$ for one element and $(i + 1)$ for the attached element. The local number for the common side of two attached quadrilaterals is i for one element and $(i + 1)$ for the other. If a quadrilateral element is attached to a triangular one, either the ith side of the quadrilateral is in common to side $(i - 1)$ of the triangle, or side $(i + 1)$ of the quadrilateral is in common to side $(i + 1)$ of the triangle. Two *sharp-edge vectors* oriented in the direction leaving from the sharp-edge vertex *bind* each sharp-edge element at the wedge. We distinguish these two vectors with the local-index number of the associated edge to indicate with $\boldsymbol{t}_\beta$ the sharp-edge vector tangent to the βth edge of a sharp-edge element. In terms of the usual edge-vector $\boldsymbol{\ell}_\beta$ [1] one has $\boldsymbol{t}_{i\pm1} = \mp\boldsymbol{\ell}_{i\pm1}$ for triangular elements, whereas for quadrilaterals one gets $\boldsymbol{t}_i = -\boldsymbol{\ell}_i$ and $\boldsymbol{t}_{i+1} = \boldsymbol{\ell}_{i+1}$.

Singular curl-conforming vector functions were derived in [18] and [19] by using the Stern–Becker transformation [13] to map a parent unit square into the triangular object-element attached to the sharp-edge. A local polar coordinate system (ρ, σ) was used to define these elements, with the radial variable ρ equal to zero on the sharp-edge vertex. A careful study of the Stern–Becker transformation proves that singular bases are not required to model singular fields in the pseudo-azimuthal direction parallel to $\rho\boldsymbol{\nabla}\sigma$, along the edges attached to the sharp-edge vertex. Along these edges, singular bases are rather required to model the correct singular behavior of the field in the direction parallel to the edge considered. The capability of modeling singular field components parallel to the pseudo-azimuthal direction $\rho\boldsymbol{\nabla}\sigma$ must not be required for the same reason that one has to allow for discontinuous normal components along the edges of regular (i.e., non singular) elements. The singular azimuthal behavior of the field will be better approximated when resorting to higher order singular vector functions, in a way similar to what happens when higher order regular bases are used to get more accurate results also for field components normal to the element edges [37].

Although the Stern–Becker transformation [13] has been used to derive singular vector functions on triangular elements, we prefer a different approach since this transformation needs to be revised when dealing with quadrilateral elements. This transformation remains of importance to construct quadrature formulas able to deal with singular vector functions.

A. Lowest Order Sharp-Edge Potentials

To model the transverse field in the neighborhood of a sharp-edge we derive irrotational singular basis functions as the gradient of scalar potential functions ϕ that vanish for $\nu = 1$ and that are identically equal to zero on all the element edges, except for the one attached to the sharp-edge. This guarantees that the gradient of each potential is exactly normal to the element edges where $\phi = 0$. The potentials are constructed so to guarantee the correct singular tangent component of their gradient along the edge where ϕ was not set to zero. At the lowest order, two sharp-edge potential functions are defined for each sharp-edge element. The triangular sharp-edge potentials are

$$\phi_{i\pm1}(\boldsymbol{r}) = \xi_{i\mp1}\left[1-(1-\xi_i)^{\nu-1}\right] \tag{4}$$

whereas, the sharp-edge potentials of quadrilaterals are

$$\phi_i(\boldsymbol{r}) = \xi_{i+2}\left(\xi_j - \xi_j^{\nu}\right) \tag{5}$$

$$\phi_j(\boldsymbol{r}) = \xi_{j+2}\left(\xi_i - \xi_i^{\nu}\right) \tag{6}$$

with $j = i+1$.

Along their associated edge β, the potentials $\phi_\beta(\boldsymbol{r})$ defined above simplify to

$$\phi_\beta(\boldsymbol{r})|_{\xi_\beta=0} = \chi - \chi^{\nu} \tag{7}$$

with

$$\chi = \begin{cases} 1-\xi_i, & \text{for potentials (4)} \\ \xi_j, & \text{for potentials (5)} \\ \xi_i, & \text{for potentials (6).} \end{cases} \tag{8}$$

The dummy variable χ introduced in (7) is linear in one parent variable and independent on the others. Along edge β, χ varies linearly from zero to unity with $\chi = 1$ on the vertex opposite to the sharp-edge vertex, and with χ vanishing at the sharp-edge vertex reached at $\xi_i = 1$ for potentials (4), $\xi_j = 0$ for potentials (5) and $\xi_i = 0$ for potentials (6).

Sharp-edge potentials readily permits one to define a C_0 continuous edge-based potential function $\psi_e(\boldsymbol{r})$ that spans two singular elements having in common the edge labeled with global index e. For example, with reference to Fig. 1, the local index for the edge common to two attached triangles is $(i-1)$ for the first element and $(i+1)$ for the second element. In this case the edge-based potential function $\psi_e(\boldsymbol{r})$ associated with the common edge e is defined as ϕ_{i-1} on the first element and as ϕ_{i+1} on the second element, with $\psi_e(\boldsymbol{r})$ given as in (7) on the common edge and $\psi_e(\boldsymbol{r}) = 0$ on the other edges. Along their associated edge, the gradient of the potentials (4)–(6) exhibits the correct singularity of Meixner theory at the sharp-edge vertex [7]. These potentials can be readily used to construct singular vector functions with a continuous tangent component along the element edges attached to the sharp-edge vertex. In fact, in general, one has:

$$\boldsymbol{t}_e \cdot \nabla\psi_e(\boldsymbol{r})|_{\text{on edge } e} = \boldsymbol{t}_\beta \cdot \nabla\phi_\beta(\boldsymbol{r})|_{\xi_\beta=0} = 1 - \nu\chi^{\nu-1} \tag{9}$$

where $\boldsymbol{t}_e$ is the sharp-edge vector relative to the eth *global* edge.

Potentials (4)–(6) are given in terms of parent coordinates for both triangular and quadrilateral elements. Their expression does not involve complex coordinate transformations. Higher order, continuous tangential, irrotational wedge-fields can be easily obtained from these results with a general simple procedure.

B. Sharp-Edge Potential Bases of Order s

We now construct higher order sharp-edge potentials by forming the product of the lowest order potentials with complete polynomial factors of order s. Although the set of polynomial factors may take different forms (and hierarchical forms are also possible), we prefer to work with the set formed by the Silvester interpolation polynomials, as already done in [1]. This choice seems to be the most convenient because: a) the Silvester interpolation polynomials do not interpolate the sharp-edge vertex or the other element vertices; b) we routinely use the same polynomial factors to construct higher order vector bases on all the remaining regular (i.e., nonsingular) elements [1].

Triangular Potentials: The interpolation polynomial factors that interest sharp-edge triangular elements are reported in Table I according to the element representation used here, although these factors are the same defined in [1]. In Table I, $R_a(q+2,\xi_i)$ indicates the interpolation Silvester polynomial of order a whereas $\widehat{R}_a(q+2,\xi_i)$ indicates the shifted interpolation Silvester polynomial of order $(a-1)$ (see [1]). The subscripts b and c are used likewise to indicate polynomials of the variable ξ_{i+1} and ξ_{i-1}, respectively.

Triangular sharp-edge potential bases of order s are defined by

$$\phi_{abc}^{i\pm1}(\boldsymbol{r}) = \alpha_{abc}^{i\pm1}(s,\boldsymbol{\xi})\phi_{i\pm1}(\boldsymbol{r}) \tag{10}$$

with $\phi_{i\pm1}(\boldsymbol{r})$ given in (4) and $\alpha_{abc}^{i\pm1}(s,\boldsymbol{\xi})$ reported in Table I. Dependency in the basis set (10) exists for $s \geq 1$ since one has $\xi_{i+1}\phi_{i+1}(\boldsymbol{r}) - \xi_{i-1}\phi_{i-1}(\boldsymbol{r}) = 0$. This dependency is easily eliminated by discarding from this set all the functions $\phi_{abc}^{i-1}(\boldsymbol{r})$ for $c = \{1, s\}$ and $a, b = \{1, s+1\}$, or all the functions $\phi_{abc}^{i+1}(\boldsymbol{r})$ for $b = \{1, s\}$ and $a, c = \{1, s+1\}$. The number of independent functions in set (10) is $(s+1)(s+4)/2$.

Continuity of the sth order sharp-edge potentials across the edge in common to adjacent elements naturally comes out from (7) and from use of interpolation polynomials. The basis set (10) is in fact able to produce, along the edges attached to the sharp-edge vertex, a representation sth order complete with respect to $(\chi - \chi^{\nu})$ as a weighting factor. These bases are necessary to represent scalar (longitudinal) fields that, at the sharp-edge vertex, vanish as ρ^{ν} times a polynomial factor of order s. In numerical applications, we use set (10) together with the *regular* polynomial set normally used to represent the unknown longitudinal field component on triangular elements.

TABLE I
SILVESTER-LAGRANGE INTERPOLATING POLYNOMIALS FOR qTH ORDER ELEMENT CONFORMITY [1]

Triangular Element - The order of each interpolating polynomial is q:

$$\begin{aligned}\alpha^{i}_{abc}(q,\boldsymbol{\xi}) &= R_a(q+2,\xi_i)\,\widehat{R}_b(q+2,\xi_{i+1})\,\widehat{R}_c(q+2,\xi_{i-1})\\ \alpha^{i+1}_{abc}(q,\boldsymbol{\xi}) &= \widehat{R}_a(q+2,\xi_i)\,R_b(q+2,\xi_{i+1})\,\widehat{R}_c(q+2,\xi_{i-1})\\ \alpha^{i-1}_{abc}(q,\boldsymbol{\xi}) &= \widehat{R}_a(q+2,\xi_i)\,\widehat{R}_b(q+2,\xi_{i+1})\,R_c(q+2,\xi_{i-1})\end{aligned}$$

with $a+b+c=q+2,\ \boldsymbol{\xi}=(\xi_i,\xi_{i+1},\xi_{i-1})$.

Quadrilateral Element - The order of each interpolating polynomial is $2q$:

$$\begin{aligned}\alpha^{i}_{ac;bd}(q,\boldsymbol{\xi}) &= R_a(q+1,\xi_i)\widehat{R}_b(q+2,\xi_{i+1})\widehat{R}_c(q+1,\xi_{i+2})\widehat{R}_d(q+2,\xi_{i-1})\\ \alpha^{i+2}_{ac;bd}(q,\boldsymbol{\xi}) &= \widehat{R}_a(q+1,\xi_i)\widehat{R}_b(q+2,\xi_{i+1})R_c(q+1,\xi_{i+2})\widehat{R}_d(q+2,\xi_{i-1})\end{aligned}$$

with $a+c=q+1,\ \ b+d=q+2,\ \boldsymbol{\xi}=(\xi_i,\xi_{i+2};\xi_{i+1},\xi_{i-1})$;

$$\begin{aligned}\alpha^{i+1}_{ac;bd}(q,\boldsymbol{\xi}) &= \widehat{R}_a(q+2,\xi_i)R_b(q+1,\xi_{i+1})\widehat{R}_c(q+2,\xi_{i+2})\widehat{R}_d(q+1,\xi_{i-1})\\ \alpha^{i-1}_{ac;bd}(q,\boldsymbol{\xi}) &= \widehat{R}_a(q+2,\xi_i)\widehat{R}_b(q+1,\xi_{i+1})\widehat{R}_c(q+2,\xi_{i+2})R_d(q+1,\xi_{i-1})\end{aligned}$$

with $a+c=q+2,\ \ b+d=q+1,\ \boldsymbol{\xi}=(\xi_i,\xi_{i+2};\xi_{i+1},\xi_{i-1})$.

$R_m(n,\xi)$ indicates the interpolation Silvester polynomial of order m in ξ, where ξ is in the interval [0,1] and where the range on the index m is $\{0,q\}$, for $m=a,b,c$ or d and $n=q+1$ or $q+2$. $\widehat{R}_m(n,\xi)$ is the shifted interpolation Silvester polynomial of order $(m-1)$ with range on the index $m=\{1,q+1\}$. The parameter n indicates the number of uniform subintervals into which the interval is divided (see [1]).

The gradient of the higher order potentials has a vanishing tangent component along the edges of the sharp-edge triangle with the following exceptions, valid for ($\beta=i+1,\ b=0,\ m=a$) and ($\beta=i-1,\ c=0,\ m=a$):

$$\boldsymbol{t}_\beta\cdot\boldsymbol{\nabla}\phi^{\beta}_{abc}(\boldsymbol{r})\Big|_{\xi_\beta=0}=\left(1-\nu\chi^{\nu-1}\right)\hat{\alpha}_m(\chi)+(\chi-\chi^{\nu})\,\frac{d\hat{\alpha}_m(\chi)}{d\chi}\quad(11)$$

with

$$\hat{\alpha}_m(\chi)=\widehat{R}_m(q,1-\chi)\widehat{R}_{q-m}(q,\chi),\qquad q=s+2,\quad m=\{1,s+1\}\quad(12)$$

and χ defined in the first of (8). The previous result generalizes (9) to higher order.

Quadrilateral Potentials: Table I reports the interpolation polynomial factors for quadrilateral elements. Quadrilateral sharp-edge potential bases of order s are defined by the following $2(s+1)^2$ independent functions

$$\begin{aligned}\phi^{i}_{ac;bd}(\boldsymbol{r})&=\alpha^{i}_{ac;bd}(s,\boldsymbol{\xi})\,\phi_i(\boldsymbol{r}),\\ \phi^{i+1}_{ac;bd}(\boldsymbol{r})&=\alpha^{i+1}_{ac;bd}(s,\boldsymbol{\xi})\,\phi_{i+1}(\boldsymbol{r})\end{aligned}\quad(13)$$

with $s\geq 0$. Once again, continuity of the sth order sharp-edge potentials across the edge in common to adjacent elements naturally comes out from (7) and from use of interpolation polynomials.

The gradients of (13) have vanishing tangent component along the edges of the sharp-edge quadrilateral with the following exceptions, valid for ($\beta=i,\ a=0,\ m=d$) and ($\beta=i+1,\ b=0,\ m=c$):

$$\boldsymbol{t}_\beta\cdot\boldsymbol{\nabla}\phi^{\beta}_{ac;bd}(\boldsymbol{r})\Big|_{\xi_\beta=0}=(1-\nu\chi^{\nu-1})\hat{\alpha}_m(\chi)+(\chi-\chi^{\nu})\frac{d\hat{\alpha}_m(\chi)}{d\chi}\quad(14)$$

with $\hat{\alpha}_m(\chi)$ given in (12) and χ defined in (8). Equation (14) generalizes (9) to arbitrarily higher order. Since the expressions on the right-hand side of (11) and (14) are equals, the tangential continuity of the gradient of higher order sharp-edge potentials across element boundaries is automatically ensured.

IV. CURL CONFORMING FUNCTIONS

To fulfill the third requirement given in Section II one has to include in the basis set singular, curl-free vector functions derived as the gradient of the scalar potential functions ϕ reported in Section III-A. The gradient of each potential is exactly normal to the element edges where $\phi=0$. Along the remaining edge where $\phi\neq 0$, the potential has been constructed so to guarantee the correct singular tangent component of the related vector function.

The last requirement of Section II leads one to include in the basis set vector functions having curl that vanishes at the edge of the wedge as ρ^{ν} [18]. These functions ought to be edgeless, that is to say with a zero-tangent component along all the edges of the element, for two reasons: a) they are primarily required to model the curl of the field solution rather than the field itself; b) they must not spoil element compatibility. Being edgeless, these functions are element-based by nature and they do not pose any problem of conformity to adjacent elements.

In the following, we use the same notation of [1] and indicate with $\boldsymbol{\Omega}$ the edge-based, regular curl-conforming functions. Conversely, sharp-edge basis functions are always identified by the presence of a superscript on the left-hand side of their symbol. The symbol is overturned for edgeless functions. For example, ${}^{\mathbf{o}}\boldsymbol{\Omega}$ indicates an edge-based singular vector function with zero curl, while ${}^{\boldsymbol{\nu}}\boldsymbol{\mho}$ is used to indicate an edgeless function having curl that at the sharp-edge vertex vanishes as ρ^{ν}.

A. Singular Curl-Conforming Bases on Triangles

Lowest Order Singular Bases: The lowest order singular triangular bases reported in Table II contain the regular zeroth-order bases $\boldsymbol{\Omega}_\beta(\boldsymbol{r})$ already discussed in [1].

The two curl-free functions ${}^{\mathbf{o}}\boldsymbol{\Omega}_{i\pm1}(\boldsymbol{r})$ vanish at $\nu=1$ and are the gradient of the scalar potentials (4), also vanishing at

TABLE II
LOWEST-ORDER CURL-CONFORMING BASES

Basis Functions	Surface Curls
Triangular Bases, with subscripts counted modulo 3, and $i = 1, 2$ or 3	
Regular Functions $\boldsymbol{\Omega}_\beta(\boldsymbol{r}) = \xi_{\beta+1}\boldsymbol{\nabla}\xi_{\beta-1} - \xi_{\beta-1}\boldsymbol{\nabla}\xi_{\beta+1}$ for $\beta = i, i \pm 1$	$\boldsymbol{\nabla} \times \boldsymbol{\Omega}_\beta(\boldsymbol{r}) = 2\,\hat{\boldsymbol{n}}/\mathcal{J}$ for $\beta = i, i \pm 1$
Wedge Functions $^{\mathbf{0}}\boldsymbol{\Omega}_{i\pm1}(\boldsymbol{r}) = \boldsymbol{\nabla}\left[\xi_{i\mp1}\left(1-\chi^{\nu-1}\right)\right]$ $^{\boldsymbol{\nu}}\boldsymbol{\mho}_i(\boldsymbol{r}) = (1-\nu)\left(\chi^\nu - 1\right)\boldsymbol{\Omega}_i(\boldsymbol{r})$ with $\chi = 1 - \xi_i$	$\boldsymbol{\nabla} \times {}^{\mathbf{0}}\boldsymbol{\Omega}_{i\pm1}(\boldsymbol{r}) = 0$ $\boldsymbol{\nabla} \times {}^{\boldsymbol{\nu}}\boldsymbol{\mho}_i(\boldsymbol{r}) = (1-\nu)\,\frac{[(2+\nu)\chi^\nu - 2]}{\mathcal{J}}\,\hat{\boldsymbol{n}}$ with $\chi = 1 - \xi_i$
Quadrilateral Bases, with subscripts counted modulo 4, and $i = 1, 2, 3$ or 4	
Regular Functions $\boldsymbol{\Omega}_\beta(\boldsymbol{r}) = \xi_{\beta+2}\boldsymbol{\nabla}\xi_{\beta-1}$ for $\beta = i, i+2, i \pm 1$	$\boldsymbol{\nabla} \times \boldsymbol{\Omega}_\beta(\boldsymbol{r}) = \frac{\hat{\boldsymbol{n}}}{\mathcal{J}}$ for $\beta = i, i+2, i \pm 1$
Wedge Functions $^{\mathbf{0}}\boldsymbol{\Omega}_i(\boldsymbol{r}) = \left(\xi_j^\nu - \xi_j\right)\boldsymbol{\nabla}\xi_i + \left(\nu\,\xi_j^{\nu-1} - 1\right)\boldsymbol{\Omega}_i(\boldsymbol{r})$ $^{\mathbf{0}}\boldsymbol{\Omega}_j(\boldsymbol{r}) = \left(\xi_i^\nu - \xi_i\right)\boldsymbol{\nabla}\xi_j - \left(\nu\,\xi_i^{\nu-1} - 1\right)\boldsymbol{\Omega}_j(\boldsymbol{r})$ $^{\boldsymbol{\nu}}\boldsymbol{\mho}_\beta(\boldsymbol{r}) = (1-\nu)\left(\xi_{\beta+2}^\nu - 1\right)\boldsymbol{\Omega}_\beta(\boldsymbol{r}),\ \ \beta = i, j$ with $j = i+1$	$\boldsymbol{\nabla} \times {}^{\mathbf{0}}\boldsymbol{\Omega}_\beta(\boldsymbol{r}) = 0$ $\boldsymbol{\nabla} \times {}^{\boldsymbol{\nu}}\boldsymbol{\mho}_\beta(\boldsymbol{r}) = (1-\nu)\frac{\left[(1+\nu)\,\xi_{\beta+2}^\nu - 1\right]}{\mathcal{J}}\,\hat{\boldsymbol{n}}$ for $\beta = i, j$ and with $j = i+1$
$\mathcal{J}$ indicates the element Jacobian and $\hat{\boldsymbol{n}}$ is the unit vector normal to the element [1].	

$\nu = 1$. These functions are associated with only one edge of the triangular element (edge $\beta = i \pm 1$), since their tangent component along the remaining two element edges is zero.

$^{\boldsymbol{\nu}}\boldsymbol{\mho}_i(\boldsymbol{r})$ inherited the subscript i from the regular function $\boldsymbol{\Omega}_i(\boldsymbol{r})$ that appears in its expression, although this function is element-based because of its vanishing tangent component along each of the three element edges. The factor $(1-\nu)$ has been introduced in the expression of $^{\boldsymbol{\nu}}\boldsymbol{\mho}_i(\boldsymbol{r})$ so to set this function to zero at $\nu = 1$, as it already happens for the functions $^{\mathbf{0}}\boldsymbol{\Omega}_{i\pm1}(\boldsymbol{r})$. In numerical applications, for ν almost equal to unity, the factor $(1-\nu)$ could be omitted to rescale the expansion coefficients to convenient values. In this connection, we recall that there is no need to normalize $^{\boldsymbol{\nu}}\boldsymbol{\mho}_i(\boldsymbol{r})$ in order to guarantee conformity to adjacent elements, since $^{\boldsymbol{\nu}}\boldsymbol{\mho}_i(\boldsymbol{r})$ is edgeless.

Completeness of Lowest Order Bases: Our bases consider only the first term of Meixner's expansion that holds in the neighborhood of the edge of the wedge for the transverse field and its curl. In fact:

1) on the βth edge, for $\beta = i \pm 1$, the tangent component $\boldsymbol{t}_\beta \cdot {}^{\mathbf{0}}\boldsymbol{\Omega}_\beta(\boldsymbol{r})$ equals $[1 - \nu\chi^{\nu-1}]$, with $\chi = 1 - \xi_i$ [see (8) and (9)].
2) the following linear combinations of our basis functions are able to represent a singular curl-free vector parallel to the basis vector $\boldsymbol{\nabla}\xi_i$, and the correct vanishing of the curl at the sharp-edge vertex, that may occur only if $\nu \neq 1$:

$$^{\mathbf{0}}\boldsymbol{\Omega}_{i+1}(\boldsymbol{r}) + \boldsymbol{\Omega}_{i+1}(\boldsymbol{r}) + {}^{\mathbf{0}}\boldsymbol{\Omega}_{i-1}(\boldsymbol{r}) + \boldsymbol{\Omega}_{i-1}(\boldsymbol{r}) = \nu(1-\xi_i)^{\nu-1}\boldsymbol{\nabla}\xi_i \tag{15}$$

$$\boldsymbol{\nabla} \times \left[{}^{\boldsymbol{\nu}}\boldsymbol{\mho}_i(\boldsymbol{r}) + (1-\nu)\boldsymbol{\Omega}_i(\boldsymbol{r})\right] = (1-\nu)\frac{(2+\nu)\,(1-\xi_i)^\nu}{\mathcal{J}}\hat{\boldsymbol{n}}. \tag{16}$$

For these reasons, as far as singular fields are concerned, the order of our basis set is $s = 0$. However, the basis set is complete to the regular zeroth-order because its regular subset $\boldsymbol{\Omega}_\beta(\boldsymbol{r})$ is complete to order zero [1]. That is to say, the basis set can model regular fields of order $p = 0$. From now on, the order of singular bases is given by a couple $[p, s]$ of integer indexes; with this notation, the order of the bases of Table II is $[0, 0]$.

Conformity of the Singular Bases of Order $[0, 0]$*:* Our basis functions are conforming to adjacent zeroth-order regular elements attached to the ith edge of the singular element, since in our bases only the regular function $\boldsymbol{\Omega}_i(r)$ has a tangent component on this edge (a constant tangent component [1]). As far as the two remaining edges $(i \pm 1)$ are concerned, conformity to adjacent elements is ensured in the usual way since the tangent component of our basis functions along their associated edge is either constant ($\boldsymbol{\Omega}_{i\pm1}$ functions) or singular ($^{\mathbf{0}}\boldsymbol{\Omega}_{i\pm1}$ functions), with the singular tangent components taking the general form given in (9). Hence, to ensure tangential continuity across element boundaries, one has only to fix the sign of these functions in accordance to the reference convention given by the orientation of the sharp-edge vectors $\boldsymbol{t}_{i\pm1}$.

Order $[p, s]$ *Bases:* Curl-conforming functions of higher order are formed by the product of the lowest order bases with complete Silvester interpolation polynomial factors. In order to obtain bases with a regular curl, the higher order static functions

associated with the static functions ${}^{\mathbf{O}}\mathbf{\Omega}_{i\pm1}$ are obtained by taking the gradient of the higher order scalar potentials (10). Higher order $[p,s]$ bases (p and $s \geq 0$) are the union of the following two sets:

$$\begin{cases} {}^{\boldsymbol{\nu}}\mathbf{\Upsilon}^{i}_{abc}(\boldsymbol{r}) = \alpha^{i}_{abc}(s,\boldsymbol{\xi})\,{}^{\boldsymbol{\nu}}\mathbf{\Upsilon}_{i}(\boldsymbol{r}) \\ {}^{\mathbf{O}}\mathbf{\Omega}^{i+1}_{abc}(\boldsymbol{r}) = \alpha^{i+1}_{abc}(s,\boldsymbol{\xi})\,{}^{\mathbf{O}}\mathbf{\Omega}_{i+1}(\boldsymbol{r}) + \phi_{i+1}(\boldsymbol{r})\nabla\alpha^{i+1}_{abc}(s,\boldsymbol{\xi}) \\ {}^{\mathbf{O}}\mathbf{\Omega}^{i-1}_{abc}(\boldsymbol{r}) = \alpha^{i-1}_{abc}(s,\boldsymbol{\xi})\,{}^{\mathbf{O}}\mathbf{\Omega}_{i-1}(\boldsymbol{r}) + \phi_{i-1}(\boldsymbol{r})\nabla\alpha^{i-1}_{abc}(s,\boldsymbol{\xi}) \end{cases} \tag{17}$$

$$\begin{cases} \mathbf{\Omega}^{i}_{abc}(\boldsymbol{r}) = \alpha^{i}_{abc}(p,\boldsymbol{\xi})\mathbf{\Omega}_{i}(\boldsymbol{r}) \\ \mathbf{\Omega}^{i+1}_{abc}(\boldsymbol{r}) = \alpha^{i+1}_{abc}(p,\boldsymbol{\xi})\mathbf{\Omega}_{i+1}(\boldsymbol{r}) \\ \mathbf{\Omega}^{i-1}_{abc}(\boldsymbol{r}) = \alpha^{i-1}_{abc}(p,\boldsymbol{\xi})\mathbf{\Omega}_{i-1}(\boldsymbol{r}) \end{cases} \tag{18}$$

defined in terms of the Silvester–Lagrange interpolation polynomials of order $q = s$ and $q = p$ given in Table I. Notice that by discarding set (17) one gets the regular pth order bases given in [1]. To get lower matrix condition numbers, it is convenient in numerical applications to normalize set (18) as explained in [1] and set (17) by multiplying each function of this latter set times the magnitude of the edge vector ℓ^{β}_{abc}. The last term on the right-hand side in the expressions of ${}^{\mathbf{O}}\mathbf{\Omega}^{i\pm1}_{abc}(\boldsymbol{r})$ is required to regularize the curl. After regularization of the curl, ${}^{\mathbf{O}}\mathbf{\Omega}^{i\pm1}_{abc}(\boldsymbol{r})$ turn out to be static, curl-free functions.

Dependency Relations at Interior Nodes and Element Conformity: For $s \geq 1$, the functions ${}^{\mathbf{O}}\mathbf{\Omega}^{i\pm1}_{abc}(\boldsymbol{r})$ are dependent. In fact, one has the following dependency relationship:

$$\nabla\left[\xi_{i+1}\phi_{i+1}(\boldsymbol{r}) - \xi_{i-1}\phi_{i-1}(\boldsymbol{r})\right] = 0. \tag{19}$$

This dependency is easily eliminated by discarding all the functions ${}^{\mathbf{O}}\mathbf{\Omega}^{i-1}_{abc}(\boldsymbol{r})$ for $c = \{1, s\}$ and $a, b = \{1, s+1\}$, or all the functions ${}^{\mathbf{O}}\mathbf{\Omega}^{i+1}_{abc}(\boldsymbol{r})$ for $b = \{1, s\}$; $a, c = \{1, s+1\}$. Similarly, as shown in [1], one has to eliminate the dependency of the regular $\mathbf{\Omega}$-functions, again by discarding all the functions $\mathbf{\Omega}^{i-1}_{abc}(\boldsymbol{r})$ for $c = \{1, p\}$; $a, b = \{1, p+1\}$, or all the functions $\mathbf{\Omega}^{i+1}_{abc}(\boldsymbol{r})$ for $b = \{1, p\}$; $a, c = \{1, p+1\}$. This simple result is of great importance since the rule used to guarantee bases independency is the same already discussed in [1].

The bases are compatible with regular pth order elements along the edge opposite to the singularity. The tangential continuity of the field along the two remaining edges of the triangular element is easily ensured by fixing the sign of the basis functions in accordance to the reference convention given by the orientation of the sharp-edge vectors $\boldsymbol{t}_{i\pm1}$ [see also (11), (12), and (14)].

In the neighborhood of the sharp-edge vertex one has $\chi \simeq 0$ and $\boldsymbol{t}_{\beta}\cdot{}^{\mathbf{O}}\mathbf{\Omega}^{\beta}_{abc}(\boldsymbol{r})\big|_{\xi_{\beta}=0} \simeq \hat{\alpha}_{a}(\chi)(1-\nu\chi^{\nu-1})$, for $\beta = i \pm 1$. It is then straightforward to prove that in the neighborhood of the sharp-edge vertex, for $s \geq 0$, the singular edge-behaviors are complete to order s with respect to $(1-\nu\chi^{\nu-1})$ as a weighting factor.

Number of Degrees of Freedom (DOF): The total number of DOF for pth order regular curl-conforming bases on a triangle is $(p+1)(p+3)$ [1]. For singular bases of order $[p,s]$, this figure has to grow as follows:

- one singular component (associated with ${}^{\mathbf{O}}\mathbf{\Omega}^{i\pm1}_{abc}$) $\times(s+1)$ DOFs $\times$ two edges $= 2(s+1)$ edge DOF;
- one singular component (associated either with ${}^{\mathbf{O}}\mathbf{\Omega}^{i+1}_{abc}$ or with ${}^{\mathbf{O}}\mathbf{\Omega}^{i-1}_{abc}$) $\times s(s+1)/2$ DOFs $\times$ one face $= s(s+1)/2$ triangle interior DOF;
- one edgeless component (associated with ${}^{\boldsymbol{\nu}}\mathbf{\Upsilon}^{i}_{abc}$) $\times(s+1)(s+2)/2$ DOFs $\times$ one face $= (s+1)(s+2)/2$ triangle interior DOF;

for a total of $(p+1)(p+3)+(s+1)(s+3)$ DOF per sharp-edge triangle.

B. Singular Curl-Conforming Bases on Quadrilaterals

With reference to Fig. 1, we assume the sharp-edge vertex located at the vertex in common to the quadrilateral edges i and $j = i+1$.

Singular Bases of Order $[0,0]$*:* The eight vector functions reported at bottom of Table II are able to correctly model the edge-field singularity on curved quadrilateral elements and define the lowest order singular bases.

The four regular zeroth-order functions $\mathbf{\Omega}_{\beta}(\boldsymbol{r})$ have already been discussed in [1]. The remaining four functions model the edge singularity and vanish for $\nu = 1$, when singular fields are not supported. The two static (curl-free) functions ${}^{\mathbf{O}}\mathbf{\Omega}_{i}(\boldsymbol{r})$, ${}^{\mathbf{O}}\mathbf{\Omega}_{j}(\boldsymbol{r})$ are the gradient of the scalar potentials (5) and (6) and are associated with edge i and j, respectively; along the remaining three element edges they have a zero tangent component.

The functions ${}^{\boldsymbol{\nu}}\mathbf{\Upsilon}_{\beta}(\boldsymbol{r})$ inherited the β subscript from the regular function $\mathbf{\Omega}_{\beta}(\boldsymbol{r})$ ($\beta = i, i+1$) appearing in their expression, although these functions are element-based because they have vanishing tangent component along each of the four element edges. In numerical applications and for ν almost equal to unity, the factor $(1-\nu)$ introduced to set ${}^{\boldsymbol{\nu}}\mathbf{\Upsilon}_{\beta}(\boldsymbol{r}) = 0$ at $\nu = 1$ could be omitted to rescale the expansion coefficients to convenient values.

Completeness and Conformity of $[0,0]$*-Order Bases:* Our bases are complete to the regular zeroth-order because the regular subset $\mathbf{\Omega}_{\beta}(\boldsymbol{r})$ is complete to order zero [1]. That is to say, the bases can model regular fields of order $p = 0$. Furthermore, the order of singularity of our bases is $s = 0$ since they are able to consider only the first term of the Meixner expansion that holds in the neighborhood of the edge of the wedge for the transverse field and its curl. In fact:

1) the correct vanishing of the curl at the sharp-edge vertex that may occur only for $\nu \neq 1$ is modeled by linear combinations of our basis functions as it follows:

$$\nabla\times\left[{}^{\boldsymbol{\nu}}\mathbf{\Upsilon}_{\beta}(\boldsymbol{r}) + (1-\nu)\mathbf{\Omega}_{\beta}(\boldsymbol{r})\right] = (1-\nu)(1+\nu)\xi^{\nu}_{\beta+2}\frac{\hat{\boldsymbol{n}}}{\mathcal{J}} \qquad \beta = i, i+1 \tag{20}$$

2) the tangent component $\boldsymbol{t}_{\beta}\cdot{}^{\mathbf{O}}\mathbf{\Omega}_{\beta}(\boldsymbol{r})$ is equal to $(1-\nu\chi^{\nu-1})$ with $\chi = \xi_{j}$ and $\chi = \xi_{i}$ on edge $\beta = i$ and $\beta = j$, respectively. Our static functions are fully compatible with the singular vector functions of a triangular element attached to the quadrilateral element at issue. The conformity of the regular subset then yields to the complete conformity of our bases to adjacent elements having order $p = 0$.

Order $[p,s]$ *Bases:* We construct higher order curl-conforming functions by applying the same technique used for

the singular triangular bases, with the necessary modifications (see [1]) required to deal with quadrilateral elements. The $[p, s]$-order bases are obtained by the union of the normalized regular set of order p given in [1] with the following Meixner set of singularity order s ($s \geq 0$ and integer), shown in (21) at the bottom of the page, defined in terms of the Silvester–Lagrange interpolation polynomials given in Table I.

Dependency Relations at Interior Nodes and Element Conformity: The functions of the Meixner subset (21) are linearly independent for all value of s. On the contrary, dependency in the regular subset exist for $p \geq 1$. To eliminate this dependency one has to discard some regular basis functions exactly as explained in [1].

After recalling (11), (12), and (14), we observe once again that the tangential continuity along the side in common to two adjacent elements is simply ensured by fixing the sign of the basis functions in accordance to some arbitrarily chosen reference convention on the common edge.

Number of DOF: On a quadrilateral, the total number of DOFs for pth order regular curl-conforming bases is $2(p+1)(p+2)$ [1]. For singular bases of order $[p, s]$, this figure has to grow as follows:

- one singular component (associated with ${}^{\mathbf{O}}\mathbf{\Omega}^{\beta}_{ac;bd}$, $\beta = i, i+1) \times (s+1)$ DOFs $\times$ two edges $= 2(s+1)$ edge DOF;
- two singular components (associated with ${}^{\mathbf{O}}\mathbf{\Omega}^{\beta}_{ac;bd}$, $\beta = i, i+1) \times s(s+1)$ DOFs $\times$ one face $= 2s(s+1)$ quadrilateral interior DOF;
- two edgeless components (associated with ${}^{\boldsymbol{\nu}}\mathbf{\mathfrak{U}}^{\beta}_{ac;bd}$, $\beta = i, i+1) \times (s+1)^2$ DOFs $\times$ one face $= 2(s+1)^2$ quadrilateral interior DOF;

for a total of $2(p+1)(p+2) + 4(s+1)^2$ DOF per sharp-edge quadrilateral.

C. Longitudinal Bases of Order $[p, s]$ for 2-D Singular Curl-Conforming Elements

Two-dimensional FEM applications require to represent the longitudinal component of the unknown field in terms of scalar bases that are given shortly by using Silvester–Lagrange interpolation polynomials. The longitudinal bases of order $[p, s]$ are constructed as the union of two sets. The first set is formed by the sharp-edge potential bases of order s given in (10) and (13) for triangular and quadrilateral elements, respectively. These functions are needed to model longitudinal fields that vanish at the sharp-edge vertex as χ^{ν} times a polynomial factor of order s, with χ given in (8). The second longitudinal set is defined by the regular independent interpolation functions usually employed in FEM applications [39]. Continuity of the longitudinal component across the edge in common to adjacent elements naturally comes out from use of interpolation polynomials.

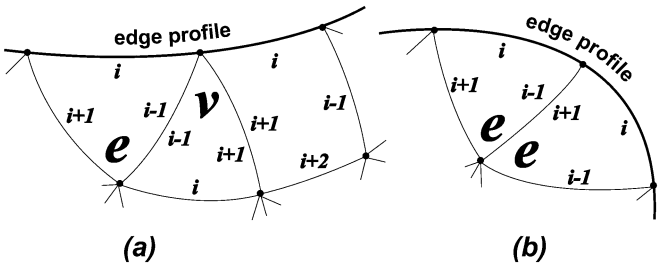


Fig. 2. (a) Local edge-numbering scheme used for edge singularity quadrilaterals and edge ($\boldsymbol{e}$) and vertex ($\boldsymbol{v}$) singularity triangles. Notice that the element edges $i \pm 1$ always depart from the edge profile. (b) Although two edge singularity triangles can have an edge in common, the basis functions cannot model a corner singularity.

As said, triangular elements require to use also the following $(p+2)(p+3)/2$ independent polynomial interpolation functions of order $(p+1)$

$$L_{abc}(\boldsymbol{r}) = R_a(p+1, \xi_i) R_b(p+1, \xi_{i+1}) R_c(p+1, \xi_{i-1}) \quad (22)$$

with $a+b+c = p+1$ and where the ranges on the indexes a, b, c are $\{0, p+1\}$. The total number of longitudinal DOF per sharp-edge triangle of order $[p, s]$ is then equal to $[(p+2)(p+3) + (s+1)(s+4)]/2$.

Conversely, the second longitudinal set to be used on quadrilateral elements is given by the following $(p+2)^2$ independent polynomial interpolation functions of order $2(p+1)$

$$L_{ac;bd}(\boldsymbol{r}) = R_a(p+1, \xi_i) R_b(p+1, \xi_{i+1}) \cdot R_c(p+1, \xi_{i+2}) R_d(p+1, \xi_{i-1}) \quad (23)$$

with $a + c = b + d = p + 1$ and where the ranges on the indexes a, b, c and d are $\{0, p+1\}$. Thus, the total number of longitudinal DOF per sharp-edge quadrilateral of order $[p, s]$ is $(p+2)^2 + 2(s+1)^2$.

V. Divergence Conforming Functions

Singular divergence conforming functions are useful to model the surface current distribution on impenetrable wedges. The wedge faces in the neighborhood of the edge profile should be meshed by using edge singularity quadrilaterals and/or two types of singularity triangles: the edge (e) and the vertex (v) singularity triangle, with local edge numbering schemes shown in Fig. 2. One has no interest in considering vertex singularity quadrilaterals since the only element-filler required to mesh in the neighborhood of the edge profile is the vertex singularity triangle.

The local edge-numbering scheme sketched in Fig. 2 has been chosen so to associate the $i \pm 1$ labels to the element edges departing from the edge profile. As already done when dealing with sharp-edge potentials, it is convenient to introduce a dummy variable χ that varies linearly from zero to unity

$$\begin{cases} {}^{\boldsymbol{\nu}}\mathbf{\mathfrak{U}}^{\beta}_{ac;bd}(\boldsymbol{r}) = \alpha^{\beta}_{ac;bd}(s, \boldsymbol{\xi}) {}^{\boldsymbol{\nu}}\mathbf{\mathfrak{U}}_{\beta}(\boldsymbol{r}) \\ {}^{\mathbf{O}}\mathbf{\Omega}^{\beta}_{ac;bd}(\boldsymbol{r}) = \boldsymbol{\nabla}\left[\alpha^{\beta}_{ac;bd}(s, \boldsymbol{\xi}) \phi_{\beta}(\boldsymbol{r})\right] = \alpha^{\beta}_{ac;bd}(s, \boldsymbol{\xi}) {}^{\mathbf{O}}\mathbf{\Omega}_{\beta}(\boldsymbol{r}) + \phi_{\beta}(\boldsymbol{r}) \boldsymbol{\nabla} \alpha^{\beta}_{ac;bd}(s, \boldsymbol{\xi}) \\ \qquad \beta = i, i+1 \end{cases} \quad (21)$$

TABLE III
LOWEST-ORDER DIVERGENCE-CONFORMING BASES

Basis Functions	Surface Divergences
Triangular Bases, with subscripts counted modulo 3, and $i = 1, 2$ or 3	
Regular Functions $\boldsymbol{\Lambda}_\beta(\boldsymbol{r}) = \frac{1}{\mathcal{J}}\left(\xi_{\beta+1}\boldsymbol{\ell}_{\beta-1} - \xi_{\beta-1}\boldsymbol{\ell}_{\beta+1}\right)$ for $\beta = i, i \pm 1$	$\boldsymbol{\nabla}\cdot\boldsymbol{\Lambda}_\beta(\boldsymbol{r}) = \frac{2}{\mathcal{J}}$ for $\beta = i, i \pm 1$
Edge Singular Functions with Singularity on Edge i ($\xi_i = 0$) ${}^e\boldsymbol{\Lambda}_{i\pm1}(\boldsymbol{r}) = \left(\xi_i^{\nu-1} - 1\right)\boldsymbol{\Lambda}_{i\pm1}(\boldsymbol{r})$ ${}^e\boldsymbol{\nabla}_i(\boldsymbol{r}) = \frac{1}{\mathcal{J}}\left(\chi_{i+1}\boldsymbol{\ell}_{i-1} - \chi_{i-1}\boldsymbol{\ell}_{i+1}\right)$ with $\chi_{i\pm1} = \xi_i\left(1 - \xi_{i\mp1}\right)^{\nu-1} - \xi_i^\nu$, and $\chi_\beta = 0$ at $\xi_\beta = 0$ for $\beta = i \pm 1$	$\boldsymbol{\nabla}\cdot{}^e\boldsymbol{\Lambda}_{i\pm1}(\boldsymbol{r}) = \frac{(1+\nu)\xi_i^{\nu-1} - 2}{\mathcal{J}}$ $\boldsymbol{\nabla}\cdot{}^e\boldsymbol{\nabla}_i(\boldsymbol{r}) = -\frac{\chi'_{i+1} + \chi'_{i-1}}{\mathcal{J}}$ with $\chi'_{i\pm1} = \frac{\mathrm{d}\chi_{i\pm1}}{\mathrm{d}\xi_i}$ $= \left(1 - \xi_{i\mp1}\right)^{\nu-1} - \nu\xi_i^{\nu-1}$
Vertex Singular Functions with Singularity on Vertex i ($\xi_i = 1$) ${}^v\boldsymbol{\Lambda}_{i\pm1}(\boldsymbol{r}) = \chi_a\,\boldsymbol{\Lambda}_{i\pm1}(\boldsymbol{r}) - \chi_b\,\boldsymbol{\Lambda}_i(\boldsymbol{r})$ ${}^v\boldsymbol{\nabla}_i(\boldsymbol{r}) = \chi_a\,\boldsymbol{\Lambda}_i(\boldsymbol{r})$ with $\chi_a = \left(1 - \xi_i\right)^{\nu-1} - 1$ $\chi_b = \frac{(1-\nu)}{\nu}\xi_i\left(1 - \xi_i\right)^{\nu-2}$	$\boldsymbol{\nabla}\cdot{}^v\boldsymbol{\Lambda}_{i\pm1}(\boldsymbol{r}) = \frac{\chi_c - 2}{\mathcal{J}}$ $\boldsymbol{\nabla}\cdot{}^v\boldsymbol{\nabla}_i(\boldsymbol{r}) = \frac{\nu\chi_c - 2}{\mathcal{J}}$ with $\chi_c = \frac{(1+\nu)}{\nu}\left(1 - \xi_i\right)^{\nu-1}$
Quadrilateral Bases, with subscripts counted modulo 4, and $i = 1, 2, 3$ or 4	
Regular Functions $\boldsymbol{\Lambda}_\beta(\boldsymbol{r}) = \frac{\xi_{\beta+2}\,\boldsymbol{\ell}_{\beta-1}}{\mathcal{J}}$ for $\beta = i, i+2, i \pm 1$	$\boldsymbol{\nabla}\cdot\boldsymbol{\Lambda}_\beta(\boldsymbol{r}) = \frac{1}{\mathcal{J}}$ for $\beta = i, i+2, i \pm 1$
Edge Singular Functions with Singularity on Edge i ($\xi_i = 0$) ${}^e\boldsymbol{\Lambda}_{i\pm1}(\boldsymbol{r}) = \left(\xi_i^{\nu-1} - 1\right)\boldsymbol{\Lambda}_{i\pm1}(\boldsymbol{r})$ ${}^e\boldsymbol{\nabla}_{i+2}(\boldsymbol{r}) = \left(\xi_i^{\nu-1} - 1\right)\boldsymbol{\Lambda}_{i+2}(\boldsymbol{r})$	$\boldsymbol{\nabla}\cdot{}^e\boldsymbol{\Lambda}_{i\pm1}(\boldsymbol{r}) = \frac{\xi_i^{\nu-1} - 1}{\mathcal{J}}$ $\boldsymbol{\nabla}\cdot{}^e\boldsymbol{\nabla}_{i+2}(\boldsymbol{r}) = \frac{\nu\xi_i^{\nu-1} - 1}{\mathcal{J}}$

along these $(i \pm 1)$ edges, with $\chi = 0$ on the edge profile and $\chi = 1$ on the vertex opposite to the edge profile. With reference to Fig. 2, one has

$$\chi = \begin{cases} 1 - \xi_i, & \text{for vertex singularity triangles} \\ \xi_i, & \text{for edge singularity elements.} \end{cases} \tag{24}$$

Being an element-filler, the vertex singularity triangle is obtained mainly by considering the first two requirements given in Section II, whereas the main duty of the edge singularity elements is to fulfill the last two requirements. In fact, as we will see shortly, irrespective of whether one considers the edge singularity triangle or quadrilateral, the divergence-free current component parallel to the edge profile (i.e., parallel to the ith edges) is modeled by the following linear combination of lowest order edge-singularity basis functions

$${}^e\boldsymbol{\Lambda}_{i+1}(\boldsymbol{r}) - {}^e\boldsymbol{\Lambda}_{i-1}(\boldsymbol{r}) + \boldsymbol{\Lambda}_{i+1}(\boldsymbol{r}) - \boldsymbol{\Lambda}_{i-1}(\boldsymbol{r}) = \frac{\boldsymbol{\ell}_i}{\mathcal{J}}\xi_i^{\nu-1} \tag{25}$$

whereas, the correct singular behavior of the charge density at $\xi_i = 0$ is modeled by the divergence of the combinations

$${}^e\boldsymbol{\Lambda}_\beta + \boldsymbol{\Lambda}_\beta, \text{ for } \beta = i \pm 1. \tag{26}$$

A. Singular Divergence-Conforming Bases on Triangles

Low-order triangular bases incorporating the singular behavior of the current density near the edge of a wedge have been derived in [24] by integrating the basis function divergence, with the correct behavior of the charge density enforced in the divergence expression. The procedure used in [24] naturally yields functions of nonadditive kind (nonsubstitutive kind), in the sense that these functions reduce to the standard (regular) zeroth-order basis functions in the limit for singularity coefficient $\nu = 1$. Our singular bases are different from those given in [24], although we use the same local edge-numbering scheme and we derived them by using the same procedure explained in [24].

Singular Bases of Order $[0,0]$*:* The lowest order bases reported in Table III contain the regular divergence-conforming bases of order $p = 0$ already discussed in [1] and reported at the top of the Table. For the edge singularity triangle, the $[0,0]$-order bases are obtained by the union of the regular set with the three edge singular functions of Table III. Similarly, for the vertex singularity triangle, the basis function set of order $[0,0]$ is the

union of the regular set with the three vertex singular functions of Table III.

Each basis function of the edge and of the vertex singular set vanishes at $\nu = 1$. The divergence of ${}^{e}\mathbf{V}_i$, ${}^{v}\mathbf{V}_i$ model the singular distribution of the charge density that comes under the condition of zero total charge over the singular triangular element. The functions ${}^{e}\mathbf{V}_i$ and ${}^{v}\mathbf{V}_i$ are therefore element-based and have a vanishing normal component along each of the three element sides. To reflect the edgeless property, the symbol used to represent ${}^{e}\mathbf{V}_i$ and ${}^{v}\mathbf{V}_i$ has been obtained by overturning $\mathbf{\Lambda}$. The subscript i still appears in these symbols merely because ${}^{v}\mathbf{V}_i$ is given in terms of $\mathbf{\Lambda}_i(\boldsymbol{r})$, whereas ${}^{e}\mathbf{V}_i$ can be formally obtained from $\mathbf{\Lambda}_i(\boldsymbol{r})$ by replacing $\xi_{i\pm1}$ with $\chi_{i\pm1}$ (defined in Table III).

The singular functions that remain are associated only with the edge quoted in their subscript, since the normal component along the other two element edges is zero. Along side β, for $\beta = i \pm 1$, the normal components of these functions can be written as

$$ {}^{e}\mathbf{\Lambda}_\beta(\boldsymbol{r}) \cdot \hat{\boldsymbol{h}}_\beta \Big|_{\xi_\beta = 0} = {}^{v}\mathbf{\Lambda}_\beta(\boldsymbol{r}) \cdot \hat{\boldsymbol{h}}_\beta \Big|_{\xi_\beta = 0} = \frac{\chi^{\nu-1} - 1}{\ell_\beta} \tag{27} $$

where $\hat{\boldsymbol{h}}_\beta$ (defined in [1]) is the unit outward normal to the element, ℓ_β is the magnitude of the edge-vector $\boldsymbol{\ell}_\beta$, and $\chi = \xi_i$, $\chi = (1 - \xi_i)$ for ${}^{e}\mathbf{\Lambda}_\beta(\boldsymbol{r})$ and ${}^{v}\mathbf{\Lambda}_\beta(\boldsymbol{r})$, respectively (see (24)). Recall that $\chi = 0$ along the edge profile shown in Fig. 2. Furthermore, one gets

$$ {}^{e}\mathbf{\Lambda}_{i\pm1}(\boldsymbol{r}) \cdot \hat{\boldsymbol{h}}_i = \frac{\xi_i - \xi_i^\nu}{\ell_i} \tag{28} $$

$$ {}^{e}\mathbf{V}_i(\boldsymbol{r}) \cdot \hat{\boldsymbol{h}}_i = \frac{\chi_{i+1} + \chi_{i-1}}{\ell_i} \tag{29} $$

with $\chi_{i\pm1}$ given in Table III. One may observe that the functions ${}^{e}\mathbf{\Lambda}_{i\pm1}$ and ${}^{e}\mathbf{V}_i$ belong to the same *family* by noticing that ${}^{e}\mathbf{V}_i \cdot \hat{\boldsymbol{h}}_i = (\xi_i - \xi_i^\nu)/\ell_i$ on the two sides $\xi_{i\pm1} = 0$, that is exactly the same result of (28).

The results (28) and (29), show that the edge singularity triangle functions can model the normal component of the edge current density that vanishes at the edge as ξ_i^ν. These bases are also able to model the *singular* behavior of the current and charge density at the ith edge of an edge singularity triangle. In fact, the singular behavior of the divergence-free current component parallel to the ith edge (i.e., parallel to $\boldsymbol{\ell}_i$) is modeled by the linear combination (25), whereas the correct singular behavior of the charge density at $\xi_i = 0$ is modeled by the divergence of the combinations (26).

Owing to (27) and because of the element conformity of the regular subset one immediately recognizes, with reference to Fig. 2, that normal continuity across element boundaries is simply enforced by adjusting the sign of the basis functions to correspond to an arbitrarily selected reference direction across adjacent elements.

Order $[p, s]$ Bases: The $[p, s]$-order bases are obtained by the union of the normalized regular vector set of order p given in [1] with a Meixner set of order s. The Meixner set is either vertex or edge singular, depending on the type of the singularity triangle one considers. These sets are obtained by forming the product of the vertex and edge singular functions given in Table III with the complete Silvester interpolation polynomial factors reported in Table I. They can be succinctly written as

$$ \begin{cases} {}^{\triangleleft}\mathbf{\Lambda}^{i\pm1}_{abc}(\boldsymbol{r}) = \alpha^{i\pm1}_{abc}(s, \boldsymbol{\xi}) {}^{\triangleleft}\mathbf{\Lambda}_{i\pm1}(\boldsymbol{r}) \\ {}^{\triangleleft}\mathbf{V}^{i}_{abc}(\boldsymbol{r}) = \alpha^{i}_{abc}(s, \boldsymbol{\xi}) {}^{\triangleleft}\mathbf{V}_i(\boldsymbol{r}) \end{cases} \tag{30} $$

where the superscript $\triangleleft$ is either equal to e or v according to the type of the singularity triangle at issue. The normal continuity across element boundaries is enforced by adjusting the sign of the basis functions to correspond to an arbitrarily selected reference direction across adjacent elements. The number of DOFs for the regular set is $(p+1)(p+3)$ [1]. Conversely, all the $3(s+1)(s+2)/2$ basis functions given in (30) are independent because the lowest order singular functions are not constrained by any dependency relation. Therefore, the total number of DOFs per singular triangle is $(p+1)(p+3) + 3(s+1)(s+2)/2$.

B. Singular Divergence-Conforming Bases on Quadrilaterals

Singular Bases of Order $[0, 0]$: Fig. 2(a) shows the local edge numbering scheme used for edge singularity quadrilaterals. The $[0, 0]$-order quadrilateral bases of Table III are the union of the four regular divergence-conforming bases of order $p = 0$ already discussed in [1] with the three edge singular functions reported at bottom of Table III.

Each basis function of the edge singular set vanishes at $\nu = 1$. The element-based function ${}^{e}\mathbf{V}_{i+2}$ has a vanishing normal component along each of the four element sides and its divergence models the singular distribution of the charge density that comes under the condition of zero total charge over the singular element. ${}^{e}\mathbf{V}_{i+2}$ inherited the subscript $i+2$ from the regular function $\mathbf{\Lambda}_{i+2}(\boldsymbol{r})$ that appears in its expression. This function models the normal component of the edge current density that vanishes at the edge as ξ_i^ν, since one has

$$ {}^{e}\mathbf{V}_{i+2}(\boldsymbol{r}) \cdot \hat{\boldsymbol{h}}_i = \frac{\xi_i - \xi_i^\nu}{\ell_i}. \tag{31} $$

The singular functions ${}^{e}\mathbf{\Lambda}_{i\pm1}(\boldsymbol{r})$ are associated only with the edge quoted in their subscript, since the normal component along the other three element edges is zero. Along side β, for $\beta = i \pm 1$, the normal components of these functions can be written as

$$ {}^{e}\mathbf{\Lambda}_\beta(\boldsymbol{r}) \cdot \hat{\boldsymbol{h}}_\beta \Big|_{\xi_\beta = 0} = \frac{\chi^{\nu-1} - 1}{\ell_\beta} \tag{32} $$

with $\chi = \xi_i$ [see (24)]. The singular behavior of the divergence-free current component parallel to the ith edge (i.e., parallel to $\boldsymbol{\ell}_i$) is modeled by the linear combination (25), whereas the correct singular behavior of the charge density at $\xi_i = 0$ is modeled by the divergence of the combinations (26).

Owing to (27) and (32), and because of the element conformity of the regular subsets one immediately recognizes, with reference to Fig. 2(a), that normal continuity across element boundaries is simply enforced by adjusting the sign of the basis functions to correspond to an arbitrarily selected reference direction across adjacent elements.

Order $[p, s]$ Bases: The $[p, s]$-order bases are obtained by the union of the normalized regular vector set of order p given in [1] with a Meixner set of order s. This latter set is obtained by forming the product of the edge singular functions given in

Table III with the complete Silvester interpolation polynomial factors reported in Table I

$$\begin{cases} {}^{e}\mathbf{\Lambda}^{i\pm1}_{ac;bd}(\boldsymbol{r}) = \alpha^{i\pm1}_{ac;bd}(s,\boldsymbol{\xi})\,{}^{e}\mathbf{\Lambda}_{i\pm1}(\boldsymbol{r}) \\ {}^{e}\mathbf{V}^{i+2}_{ac;bd}(\boldsymbol{r}) = \alpha^{i+2}_{ac;bd}(s,\boldsymbol{\xi})\,{}^{e}\mathbf{V}_{i+2}(\boldsymbol{r}). \end{cases} \tag{33}$$

As explained in [1], the dependency in the regular subset for $p \geq 1$ is easily eliminated by discarding some regular basis functions. Similarly, the dependency of the singular edge functions for $s \geq 1$ is eliminated by discarding all the functions ${}^{e}\mathbf{\Lambda}^{i+1}_{ac;bd}(\boldsymbol{r})$ for $b = \{1, s\}$; $a, c, d = \{1, s+1\}$, or all the functions ${}^{e}\mathbf{\Lambda}^{i-1}_{ac;bd}(\boldsymbol{r})$ for $d = \{1, s\}$; $a, b, c = \{1, s+1\}$. Hence, the total number of DOFs per singular quadrilateral is $2(p+1)(p+2) + (s+1)(2s+3)$.

VI. Numerical Results

The benefits of using higher order singular vector bases are illustrated in short by showing FE results for cylindrical homogeneous waveguides. The problem is formulated in terms of the electric field as in [37]. The Galerkin form of the FEM is used to reduce the transverse vector Helmholtz problem into a generalized eigenvalue problem solved by use of an iterative method [37]. Our C++ object-oriented code computes the modal longitudinal wavenumbers k_z at a given frequency f as well as the modal fields. A symbolic representation of the singular FEM integrals is implemented to integrate the singular functions by adding up analytic integral results. This technique is highly effective and does not require complex programming to provide integral results to machine precision. Numerical Gauss–Kronrod integration [40] of the singular functions based on the Stern–Becker mapping of the triangular element into a rectangular element yields slightly less accurate results.

We first consider the circular vaned waveguide already studied in [19], that is a circular homogeneous waveguide of radius a with a zero-thickness radial vane extending to its center. The normalized waveguide dimension is $k_o a$, where k_o is the free-space wavenumber. The zeroes of the Bessel functions $J_{m/2}$ of half-integer order, and of the derivatives of these Bessel functions yield the TM and TE eigenvalues, respectively [41], [42]. The first subscript labeling these modes is m; the second subscript n indicates the order of the zero, as usual. Even values of m correspond to modes supported also by a circular waveguide, although the vane suppresses all the TM_{0n} circular waveguide modes. The modal fields exhibiting a $\nu = 1/2$ singularity at the edge of the vane are those of the TE_{1n} and the TM_{1n} modes, and the singular TE_{11} mode is dominant. A mode is defined to be singular when its eigenfield exhibits singular behavior. The numerically obtained transverse electric field topographies of the first two singular modes are reported in Fig. 3. Fig. 4 reports the percentage error in the computed square values k_z^2 of the longitudinal wavenumbers versus the number of unknowns. In Fig. 4(a) the error is averaged over the first twenty modes, which involve four singular modes. Fig. 4(b) shows the error averaged over the first four singular modes. These results have been obtained by using five different meshes, with meshes from A to D shown in the inset of Fig. 4(a). Mesh E (not shown) consists of only six curved triangular elements having as a common vertex the sharp-edge vertex. Notice that all the used meshes have six triangular elements attached to the sharp-edge vertex. As a matter of fact, Fig. 4 shows the effects obtained by trying bases of different singular s-order only on these six sharp-edge elements. For these meshes, the number of DOFs always increases by 16 when one switches regular elements to $s = 0$ singular order elements; by 34 when passing from $s = 0$ to $s = 1$, and by 86 when passing from $s = 0$ to $s = 2$. The relatively small increase in the number of DOFs associated with the use of singular elements is highly rewarded by the numerical result improvements. In fact the regular element results of Fig. 4, although obtained by using fifth-order elements, are always worse than the results provided by using singular elements.

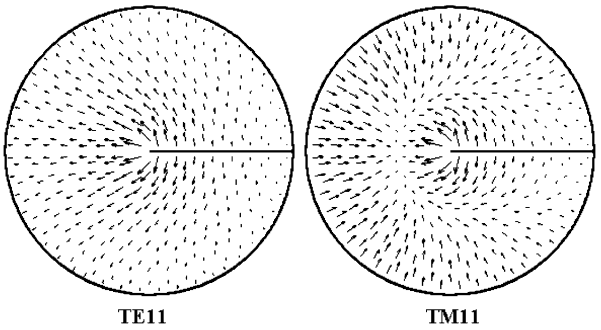


Fig. 3. Transverse electric field component of the first two singular modes supported by the circular vaned waveguide. The field associated with the dominant TE_{11} mode is reported at left. The electric field associated with the singular TM_{11} mode (fifth mode) is reported at right.

Fig. 5 shows the normalized matrix fill-in time versus the number of extra DOFs required to study the problems of Fig. 4 with singular elements and for $p = 3$. These results show that the technique used to integrate the singular functions has usually no-impact on the cpu-time required to fill-in the FEM matrices, unless singular elements are a good percentage of all elements.

Singular elements provides a noticeable improvement also in the regular mode results, since any lack of precision in the stiffness matrix coefficients yields to errors on all modes. For example, Fig. 6 reports the A-mesh percentage error in the computed square value k_z^2 of the longitudinal wavenumber for each of the first twenty modes of the circular vaned waveguide. By comparison with the results obtained when using elements of ($p = 3$, $s = 0$) order one may notice that use of regular ($p = 5$) elements yields to higher errors in the singular (TE_{1n}, TM_{1n}) as well as in the nonsingular mode results.

The second problem we consider is a circular waveguide of radius a with two radial vanes of thickness equal to $a/50$ facing each other along a diameter. The vane separation gap is centered and its width is again $a/50$. The singularity coefficient for this case is $\nu = 2/3$. Although analytical results for this waveguide are not available, we studied it to show the ability of our singular bases to handle cases where sharp-edge elements of a given wedge are bordered by sharp-edge elements of a different wedge, and also to prove the effectiveness of singular elements in dealing with thick layers.

We discretized the waveguide cross-section with 374 triangular elements and got four sharp-edge elements for each vane-wedge, for a total of 16 sharp-edge elements in the gap region. The mesh is quite dense in the gap region and rather coarse out of

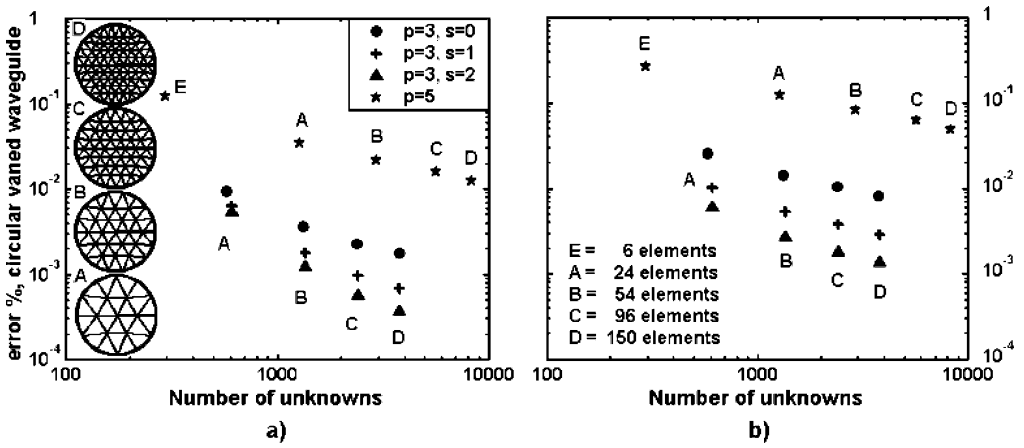


Fig. 4. Percentage errors for the first modes of the circular vaned waveguide at $k_o a = 11$. (a) Average error on the first twenty modes and (b) average error on the first four singular modes.

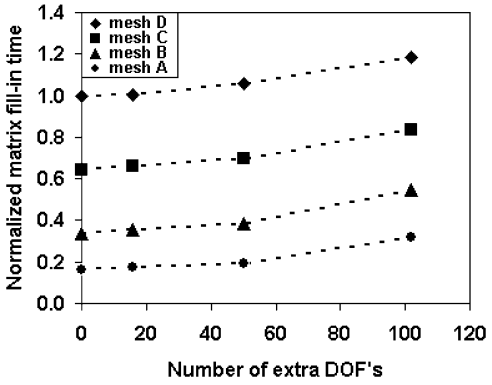


Fig. 5. Matrix fill-in time versus the number of the extra DOFs required to study with *singular* elements and for $p = 3$ the circular vaned waveguide problems of Fig. 4. The times are normalized with respect to the cpu-time t_D spent by our sparse-solver in filling-in the D-mesh FEM matrices by using only *regular* elements of order $p = 3$. Our object-oriented code yields $t_D = 65.6$ seconds on a Pentium IV Xeon@2.4 GHz machine. The number of extra DOFs is zero for the *regular* $p = 3$ cases that correspond to 3741, 2369, 1309, 561 DOFs for mesh D, C, B and A, respectively. For all the used meshes, the number of extra DOFs is 16, 50, and 102 for $s = 0$, 1 and 2, respectively.

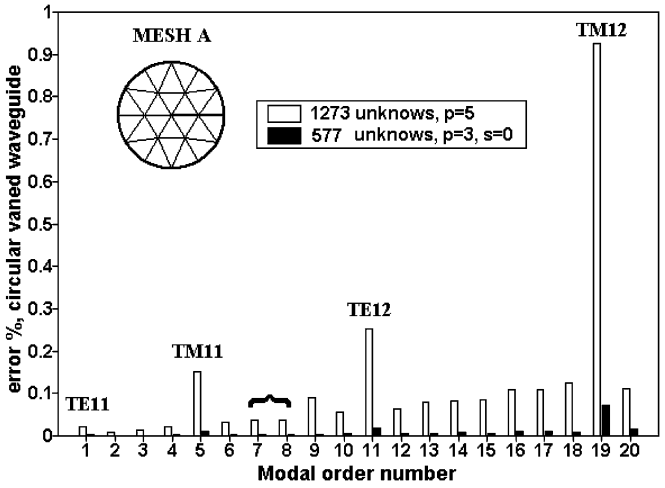


Fig. 6. Percentage error in the computed square value of the longitudinal wavenumber (k_z^2) for each of the first twenty modes of the circular vaned waveguide at $k_o a = 11$. The modes expressly labeled in the figure exhibit a singular field at the edge of the vane. Mode 7 and 8 have the same cutoff frequency since they correspond to the TM_{11} and the TE_{01} modes of the circular waveguide.

it. The results reported have been obtained by setting $k_o a = 11$, with $p = 2$ (regular elements, 5419 unknowns) and with $p = 2$, $s = 0$ (5459 unknowns). We estimated the errors by considering as reference results those obtained by setting on the same mesh $p = 3$, $s = 2$ (9733 unknowns).

Fig. 7 shows in the near-gap region both the used mesh and the numerically obtained transverse electric field topographies of the first two modes supported by this waveguide. Notice that out of 16 sharp-edge elements four have a side in common with a sharp-edge element of a different wedge, while eight more have a vertex in common with a sharp-edge element of a different wedge. The second mode of this waveguide is the dominant TE_{11} mode of the circular waveguide almost in every respect, with a distorted field topography only in the gap region. Conversely, all the energy of the dominant mode of the double-vaned waveguide is concentrated in the gap region so that it turns out that the dominant mode is quasi-TEM.

The percentage error in the computed square value k_z^2 of the longitudinal wavenumber for each of the first ten modes of the circular double-vaned waveguide is reported in Fig. 8 in natural as well as in logarithmic scale. As said, the errors have been computed by choosing as a reference the values obtained by running the code with $p = 3, s = 2$. Once again, one notices that regular bases yield higher errors than singular bases. In this case, 40 extra DOFs are required to switch from regular to singular bases of zero s-order.

VII. Conclusion

This paper presents singular curl- and divergence-conforming vector bases that incorporate the edge conditions and should provide more accurate and efficient numerical solutions of both surface integral and differential problems. Functions of arbitrarily high order are described in a unified and consistent manner for curved triangular and quadrilateral elements. Properties of the vector basis functions are discussed and these functions are proved to be fully compatible with the standard, high-order regular vector functions used in adjacent elements. Sample numerical results confirm the faster convergence of our singular higher order bases on wedge problems.

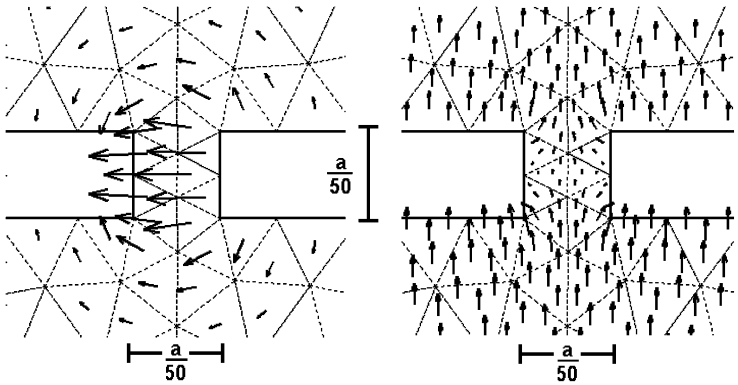


Fig. 7. Transverse electric field component in the near-gap region of the first two modes supported by the circular double-vaned waveguide of radius a. The field of the dominant singular mode is reported at left. The field associated with the second mode is given at right.

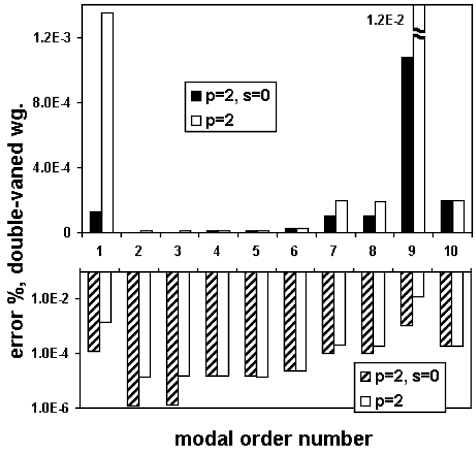


Fig. 8. Percentage error in the computed square value of the longitudinal wavenumber (k_z^2) for each of the first ten modes of the circular double-vaned waveguide at $k_o a = 11$. Errors are reported in natural scale at top and in logarithmic scale at bottom. In this case, only 40 extra DOFs are required to switch regular $(p = 2)$ elements to $(s = 0)$ singular order elements. The $(p = 2)$ regular case corresponds to 5419 DOFs.

It is hoped that the unified notation developed herein will facilitate the use of these functions in numerical electromagnetics computer codes.

REFERENCES

[1] R. D. Graglia, D. R. Wilton, and A. F. Peterson, "Higher order interpolatory vector bases for computational electromagnetics, special issue on advanced numerical techniques in electromagnetics," *IEEE Trans. Antennas Propagat.*, vol. 45, pp. 329–342, Mar. 1997.

[2] R. D. Graglia, D. R. Wilton, A. F. Peterson, and I.-L. Gheorma, "Higher order interpolatory vector bases on prism elements," *IEEE Trans. Antennas Propagat.*, vol. 46, pp. 442–450, Mar. 1998.

[3] R. D. Graglia and I.-L. Gheorma, "Higher order interpolatory vector bases on pyramidal elements," *IEEE Trans. Antennas Propagat.*, vol. 47, pp. 775–782, May 1999.

[4] S. Kato and M. Kobayashi, "Magnetic charge densities around edges of circular cylinders," *IEEE Trans. Magn.*, vol. 32, pp. 1880–1887, May 1996.

[5] K. Ozaki, M. Kobayashi, and G. Rowlands, "Surface magnetic charge distribution of a long, thin cylinder and its edge singularity," *IEEE Trans. Magn.*, pt. 2, vol. 34, pp. 2185–2191, July 1998.

[6] J. Van Bladel, *Singular Electromagnetic Fields and Sources*. Oxford, U.K.: Clarendon, 1991.

[7] J. Meixner, "The behavior of electromagnetic fields at edges," *IEEE Trans. Antennas Propagat.*, vol. AP-20, pp. 442–446, July 1972.

[8] J. Van Bladel, "Field singularities at metal-dielectric wedges," *IEEE Trans. Antennas Propagat.*, vol. AP-33, pp. 450–455, Apr. 1985.

[9] B. Khayatian, Y. Rahmat-Samii, and P. Y. Ufimtsev, "On the question of the imposition of the singular edge current behavior," in *Proc. IEEE AP-S Int. Symp.*, vol. 3, 2000, pp. 1558–1561.

[10] D. Giannacopoulos and S. McFee, "Toward optimal h-p adaptation near singularities in finite element electromagnetics," *IEEE Trans. Magn.*, pt. 2, vol. 30, pp. 3523–3526, Sept. 1994.

[11] P. S. Fridberg and I. M. Yakover, "A procedure for defining behavior of weight functions near the edge for best convergence using the Galerkin method," *IEEE Trans. Microwave Theory Tech.*, vol. 40, no. 8, pp. 1661–1666, Aug. 1992.

[12] P. A. A. Laura, C. A. Rossit, and D. V. Bambill, "Comments on 'A procedure defining behavior of weight functions near the edge for best convergence using the Galerkin method' by P.S. Fridberg and I.M. Yakover," *IEEE Trans. Microwave Theory Tech.*, vol. 41, no. 5, pp. 900–901, May 1993.

[13] M. Stern and E. B. Becker, "A conforming crack tip element with quadratic variation in the singular fields," *Int. J. Numer. Methods Eng.*, vol. 12, pp. 279–288, 1978.

[14] J. P. Webb, "Finite element analysis of dispersion in waveguides with sharp metal edges," *IEEE Trans. Microwave Theory Tech.*, vol. 36, no. 12, pp. 1819–1824, Dec. 1988.

[15] R. Miniowitz and J. P. Webb, "Covariant-projection quadrilateral elements for the analysis of waveguides with sharp edges," *IEEE Trans. Microwave Theory Tech.*, vol. 39, no. 3, pp. 501–505, Mar. 1991.

[16] J. M. Gil and J. Zapata, "Efficient singular element for finite element analysis of quasi-TEM transmission lines and waveguides with sharp metal edges," *IEEE Trans. Microwave Theory Tech.*, vol. 42, pp. 92–98, Jan. 1994.

[17] ——, "A new scalar transition finite element for accurate analysis of waveguides with field singularities," *IEEE Trans. Microwave Theory Tech.*, vol. 43, pp. 1978–1982, Aug. 1995.

[18] J. M. Gil and J. P. Webb, "A new edge element for the modeling of field singularities in transmission lines and waveguides," *IEEE Trans. Microwave Theory Tech.*, pt. 1, vol. 45, pp. 2125–2130, Dec. 1997.

[19] Z. Pantic-Tanner, J. S. Savage, D. R. Tanner, and A. F. Peterson, "Two-dimensional singular vector elements for finite-element analysis," *IEEE Trans. Microwave Theory Tech.*, vol. 46, pp. 178–184, Feb. 1998.

[20] J. S. Juntunen and T. D. Tsiboukis, "On the FEM treatment of wedge singularities in waveguide problems," *IEEE Trans. Microwave Theory Tech.*, vol. 48, pp. 1030–1037, June 2000.

[21] D. R. Wilton and S. Govind, "Incorporation of edge conditions in moment method solutions," *IEEE Trans. Antennas Propagat.*, vol. AP-25, pp. 845–850, 1977.

[22] J. Sercu, N. Fache, F. Libbrecht, and D. De Zutter, "Full-wave space-domain analysis of open microstrip discontinuities including the singular current-edge behavior," *IEEE Trans. Microwave Theory Tech.*, vol. 41, pp. 1581–1588, Sept. 1993.

[23] T. Andersson, "Moment-method calculations on apertures using basis singular functions," *IEEE Trans. Antennas Propagat.*, vol. 41, pp. 1709–1716, Dec. 1993.

[24] W. J. Brown and D. R. Wilton, "Singular basis functions and curvilinear triangles in the solution of the electric field integral equation," *IEEE Trans. Antennas Propagat.*, vol. 47, pp. 347–353, Feb. 1999.
[25] K. B. Whiting, "A treatment for boundary singularities in finite difference solutions of Laplace's equation," *IEEE Trans. Microwave Theory Tech.*, vol. MTT-16, pp. 889–891, 1968.
[26] G. Mür, "The modeling of singularities in the finite-difference approximation of the time-domain electromagnetic-field equations," *IEEE Trans. Microwave Theory Tech.*, vol. MTT-29, pp. 1073–1077, Oct. 1981.
[27] F. Bogelsack and I. Wolff, "Application of a projection method to a mode-matching solution for microstrip lines with finite metallization thickness," *IEEE Trans. Microwave Theory Tech.*, vol. MTT-35, pp. 918–921, Oct. 1987.
[28] L. Cascio, G. Tardioli, T. Rozzi, and W. J. R. Hoefer, "A quasistatic modification of TLM at knife edge and 90° wedge singularities," *IEEE Trans. Microwave Theory Tech.*, pt. 2, vol. 44, pp. 2519–2524, Dec. 1996.
[29] P. Przybyszewski and M. Mrozowski, "A conductive wedge in Yee's mesh," *IEEE Microwave Guided Wave Lett.*, vol. 8, pp. 66–68, Feb. 1998.
[30] H.-M. Chen and Y.-S. Xu, "Incorporation of the field singularity behaviors at edges into the finite-difference solution of waveguide modes," in *Proc. IEEE AP-S Int. Symp.*, vol. 2, 1998, pp. 1250–1253.
[31] A. Frenkel, "On entire-domain basis functions with square-root edge singularity," *IEEE Trans. Antennas Propagat.*, vol. 37, pp. 1211–1214, Sept. 1989.
[32] Z. Altman, D. Renaud, and H. Baudrand, "On the use of differential equations of nonentire order to generate entire domain basis functions with edge singularity," *IEEE Trans. Microwave Theory Tech.*, vol. 42, pp. 1966–1972, Oct. 1994.
[33] V. Daniele and P. L. E. Uslenghi, "Wiener-Hopf Solutions for right isorefractive wedges," Dipartimento di Elettronica, Politecnico di Torino, Internal Rep. ELT-2000-2, 2000.
[34] R. D. Graglia and G. Lombardi, "Higher-order vector bases for singular fields on curved 2D-elements," in *Proc. IEEE AP-S Symp. and USNC/CNC/URSI North Amer. Radio Science Meet., URSI Dig.*, Columbus, OH, June 2003, pp. 348–348.
[35] ——, "New higher order two-dimensional singular elements for FEM and MOM applications," in *Proc. ICEAA03*, Torino, Italy, Sept. 2003, pp. 87–89.
[36] G. Lombardi, "Implementation of higher order two-dimensional singular elements in FEM codes and numerical results," in *Proc. ICEAA03*, Torino, Italy, Sept. 2003, pp. 91–94.
[37] P. Savi, I.-L. Gheorma, and R. D. Graglia, "Full-wave high-order FEM model for lossy anisotropic waveguides," *IEEE Trans. Microwave Theory Tech.*, vol. 50, pp. 495–500, Feb. 2002.
[38] R. D. Graglia and G. Lombardi, "Vector functions for singular fields on curved triangular elements, truly defined in the parent space," in *Proc. IEEE AP-S Int. Symp.*, vol. 1, San Antonio, TX, June 2002, pp. 62–65.
[39] P. P. Silvester and R. L. Ferrari, *Finite Elements for Electrical Engineers*. Cambridge, U.K.: Cambridge Univ. Press, 1996.
[40] R. Piessens, E. de Doncker-Kapenga, C. W. Überhuber, and D. K. Kahaner, *QUADPACK: A Subroutine Package for Automatic Integration*, ser. Springer series in Computational Mathematics. Berlin: Springer-Verlag, 1983.
[41] F. E. Borgnis and C. H. Papas, "Electromagnetic waveguides and resonators," in *Encyclopedia of Physics*, S. Flügge, Ed. Berlin: Springer-Verlag, 1958, vol. XVI, Electric Fields and Waves.
[42] L. Felsen and N. Marcuvitz, *Radiation and Scattering of Waves*. Englewood Cliffs, NJ: Prentice Hall, 1973.



Roberto D. Graglia (S'83–M'83–SM'90–F'98) was born in Turin, Italy, on July 6, 1955. He received the Laurea degree (*summa cum laude*) in electronic engineering from the Polytechnic of Turin in 1979, and the Ph.D. degree in electrical engineering and computer science from the University of Illinois at Chicago in 1983.

From 1980 to 1981, he was a Research Engineer at CSELT, Italy, where he conducted research on microstrip circuits. From 1981 to 1983, he was a Teaching and Research Assistant at the University of Illinois at Chicago. From 1985 to 1992, he was a Researcher with the Italian National Research Council (CNR), where he supervised international research projects. In 1991 and 1993, he was Associate Visiting Professor at the University of Illinois at Chicago. In 1992, he joined the Department of Electronics, Polytechnic of Turin, as an Associate Professor, where, since 1999 he has been a Professor of Electrical Engineering. He has authored over 150 publications in international scientific journals and symposia proceedings. His areas of interest comprise numerical methods for high- and low-frequency electromagnetics, theoretical and computational aspects of scattering and interactions with complex media, waveguides, antennas, electromagnetic compatibility, and low-frequency phenomena. He has organized and offered several short courses in these areas.

Since 1997, he has been a Member of the editorial board of *Electromagnetics*. He is a past Associate Editor of the IEEE TRANSACTIONS ON ANTENNAS AND PROPAGATION and the IEEE TRANSACTIONS ON ELECTROMAGNETIC COMPATIBILITY. He is currently an Associate Editor of the IEEE ANTENNAS AND WIRELESS PROPAGATION LETTERS, and a Reviewer for several international journals. He was the Guest Editor of a special issue on Advanced Numerical Techniques in Electromagnetics for the IEEE TRANSACTIONS ON ANTENNAS AND PROPAGATION in March 1997. He has been Invited Convener at URSI General Assemblies for special sessions on Field and Waves in 1996, Electromagnetic Metrology in 1999, and Computational Electromagnetics in 1999. He served the International Union of Radio Science (URSI) for the triennial International Symposia on Electromagnetic Theory as Organizer of the Special Session on Electromagnetic Compatibility in 1998 and was the co-organizer of the special session on Numerical Methods in 2004. Since 1999, he has been the General Chairperson of the biennial International Conference on Electromagnetics in Advanced Applications (ICEAA), held in Turin.



Guido Lombardi (S'02–M'04) was born in Florence, Italy, on December 8, 1974. He received the Laurea degree (*summa cum laude*) in telecommunications engineering from the University of Florence, Florence, Italy, in 1999 and the Ph.D. degree in electronics engineering fron the Polytechnic of Turin, Turin, Italy, in January 2004. His Ph.D. work focused on the study of analytical and numerical aspects of electromagnetic singularities.

From 2000 to 2001, he was an Officer of the Italian Air Force. His research areas comprise numerical methods for electromagnetics, theoretical and computational aspects of FEM, waveguide problems, microwave passive components and project of orthomode transducers (OMT).

Dr. Lombardi received the Raj Mittra Travel Grant Award, as a junior researcher, at the 2003 IEEE AP-S International Symposium and USNC/CNC/URSI National Radio Science Meeting, Columbus, OH. He served as a member of the Organizing Committee of the International Conference on Electromagnetics in Advanced Applications (ICEAA), Turin, for the 2001 and 2003 editions.